Magnetic and electronic characterization of highly Co-doped ZnO: An annealing study at the solubility limit

R. Knut,[1] J. M. Wikberg,[2] K. Lashgari,[3] V. A. Coleman,[3] G. Westin,[3] P. Svedlindh,[2] and O. Karis[1]
[1]*Department of Physics, Uppsala University, P.O. Box 530, SE-751 21 Uppsala, Sweden*
[2]*Department of Engineering Sciences, Uppsala University, P.O. Box 534, SE-751 21 Uppsala, Sweden*
[3]*Department of Materials Chemistry, Uppsala University, P.O. Box 538, SE-751 21 Uppsala, Sweden*
(Received 9 March 2010; revised manuscript received 13 August 2010; published 23 September 2010)

We report on investigations of the electronic structure and magnetic properties of ZnO doped with 15 at. % Co and postgrowth annealed at temperatures ranging between 250 and 800 °C. In particular, we demonstrate how the presence of Co^{3+}, indicative of secondary phases, is manifested in spectroscopy. Through resonant photoemmision spectroscopy we have found that x-ray diffraction in some cases underestimates or does not reveal the presence of secondary phases, possibly due to unrelaxed structures or structural arrangements with sizes below the detection limit. The magnetic properties are in most cases understood by assuming small antiferromagnetic clusters but can also show a behavior indicative of ferromagnetic interactions.

DOI: 10.1103/PhysRevB.82.094438 PACS number(s): 75.50.Pp, 75.70.−i, 78.70.Dm, 79.60.−i

I. INTRODUCTION

A number of questions regarding the magnetic properties of dilute magnetic semiconductor (DMS) systems have been raised, and many attempts to understand the influence of both extrinsic and defect induced *n* doping on the magnetic properties of transition-metal-doped ZnO have been made.[1–3] Today, there is a general agreement that the properties of these materials are strongly dependent on the magnetic and chemical configuration of the dopant atoms.[4,5] There have been many reports of ferromagnetism (FM) (even at room temperature) for many different DMS systems but the extracted magnetic moments are in most cases very small compared to the expected magnetic moment of the dopant atom.[2,3,6–9] In some cases, this magnetic response has been assigned to metallic clusters[10] too small to be observed with x-ray diffraction (XRD) or too distant from the sample surface to be observed with microscopy or spectroscopy.[11,12] The question which is always raised is whether the material is phase pure or not. All characterization methods have limitations and even though several complementary techniques may be employed, it can be difficult to eliminate all doubts concerning the purity of a sample. This shows the importance of this question and the necessity of studying samples on the borderline of phase/nonphase pure to enable phase pure samples to be identified with high certainty. Every growth and preparation method has a characteristic dopant solubility limit before impurity phases are observed. According to Straumal *et al.*,[13] the solubility limit of Co in ZnO single crystals is low, between 2 and 10 at. % for heat treatments between 550 and 950 °C. They also conducted a case study of Co-doped ZnO which reveals that the solubility limit is strongly connected to the grain size of the sample, or more explicitly to the number of grain boundaries. A larger amount of grain boundaries results in a higher solubility limit. Furthermore, their suggested model for Co accumulating at grain boundaries was off by an order of magnitude when compared to experimental results. It was also shown that 10 nm grains can dissolve at most 33 at. % Co, although secondary phases in XRD were not observed until 40 at. % Co doping. It is conceivable that many experiments have been performed just below the solubility limit, obtained from XRD data, in order to maximize the measured magnetic moment. In this study we focus on the electronic structure and magnetic properties of Co-doped ZnO at the solubility limit.

II. EXPERIMENTAL DETAILS

The samples used in this study were ZnO doped with 15 at. % Co fabricated through solution-based alkoxide chemistry, using methoxy-ethanol:toluene as solvent. All manipulation of the alkoxide solutions and the films prior to heat treatment was performed in an Ar filled glove box (MBraun 200). Details of the synthesis of the alkoxide precursors is described elsewhere.[14–16] 15 at. % Co solution was prepared by mixing of Co-methoxyethoxide solution with Zn-methoxyethoxide and adjusting the total metal concentration to 0.3 M. Films were deposited on (100) Si/SiO_2 (*n* doped, 0.1 Ω cm) by dip coating yielding a total thickness of 210 nm (≈105 nm on each side of the substrate). Hydrolysis was achieved by transferring the coated substrate into a sealed flask and adding one drop of degassed (O_2 and CO_2-free) water onto the flask wall. The flask was left to stand overnight for hydrolysis. It was then evacuated to 2 Pa and heated to 150 °C for 15 min before the sample was exposed to ambient atmosphere. Postannealing was performed in a closed quartz tube furnace. The samples were annealed for 15 min in Ar atmosphere at 400, 500, 600, and 800 °C. Before heating the tube was flushed with Ar (<1 ppm O_2) at 2 L min^{-1} for 30 min before the flow was decreased to 0.1 L min^{-1}. Cooling was performed under Ar flow at 20 °C min^{-1}. A small air leakage was expected in this setup and therefore the O_2 partial pressure is somewhat higher than what is expected solely from O_2 residuals in the Ar gas. A reference ZnO sample was also fabricated and annealed at 600 °C. An as-prepared sample was reserved and is henceforth referred to as the 150 °C sample. A second set of identical samples (except for the 500 °C sample) was prepared for magnetic measurements using a thinner Si/SiO_2

substrate. The film was deposited on both sides of the substrate to increase the film to substrate magnetic moment ratio. Grazing incidence XRD was performed with an Siemens D5000 diffractometer with parallel plate geometry. Only the sample set used for spectroscopic measurements was characterized by XRD.

X-ray photoemission spectroscopy (XPS), resonant x-ray photoemission spectroscopy (RPES), and x-ray absorption spectroscopy studies were performed at beamline D1011 at MAXLAB in Lund. Absorption spectra were measured in total electron yield. The samples were in electrical contact with an Au foil from which a Fermi edge was measured after every XPS spectrum for energy calibration. Prior to spectroscopic measurements, the sample denoted 150 °C-Vac was heated *in situ* to 150 °C, i.e., the same temperature as used in the synthesis. At this point a data set for this sample was obtained. Subsequently this and all other samples were heated to 250 °C *in situ* to further desorb physisorbed surface adsorbates. Data recorded for the previously denoted 150 °C-Vac sample after heating to 250 °C are consequently denoted correspondingly (250 °C-Vac). After the heat treatment, XPS reveals that small amounts of carbon are present for all samples. Magnetic measurements were performed in a Quantum Design MPMS-XL superconducting quantum interference device magnetometer. Magnetization (M) versus temperature (T) was studied between 2 and 390 K, following two different protocols; zero-field cooled (ZFC) and field cooled (FC). The ZFC magnetization was obtained by cooling the sample to 2 K in zero field, turning on a magnetic field of 500 Oe and measuring the magnetization as the sample warmed up. The FC magnetization was subsequently obtained by measuring the magnetization, in the same applied field, as the sample cooled to 2 K. Isothermal magnetization measurements were performed at 2 K; the M versus applied field (H) was measured in the field range ± 30 kOe. It should be emphasized that the samples used for magnetic measurements were all heat treated in Ar atmosphere and did not receive any additional heating in vacuum. While the authors argue that this difference is immaterial to the samples heated to temperatures above 250 °C (i.e., 400, 600, and 800 °C), it is prudent to make distinction between the 150 and 250 °C heated in vacuum and in Ar. To make this difference clear we denote the samples heated solely in Ar: 150 °C-Ar and 250 °C-Ar.

III. RESULTS AND DISCUSSION

A main motivation of this investigation was to synthesize and study phase pure ZnO samples with a high level of Co doping over a wide range of annealing temperatures. XRD investigations using different Co concentrations and annealing temperatures suggested that phase pure samples with Co doping as high as 15% could be produced.

The temperature-dependent magnetization measurements (ZFC/FC magnetization, not shown) reveal a paramagneticlike behavior with no sign of spin ordering or superparamagnetic blocking. From magnetization (M) versus magnetic field (H) measurements, shown in Fig. 1, all samples exhibit a linear low-field dependence with no remanent magnetization or coercivity. The magnetization saturates in the high-field region, typically at some tens of kOe, except for the 400 °C sample which reaches magnetic saturation at much lower fields. In the high-field region, the variation in the diamagnetic signal from the substrate dominates over the paramagnetic signal for the 400 °C sample. This makes the extracted magnetic moments unreliable at high fields and therefore we have chosen to exclude high-field magnetic data for this sample. From the low-field slope of the M versus H curves, effective magnetic moments (μ_{eff}) have been extracted (given in Table I) with values deviating significantly from the value ($3\mu_B$) expected for tetrahedrally coordinated Co^{2+}. Comparing μ_{eff} with magnetic moments extracted from the saturation magnetization (μ_{HF}) a large discrepancy is seen, which together with the very small μ_{HF} values, indicates that small antiferromagnetic (AFM) clusters with uncompensated spins are the source of the magnetic behavior for the 150 °C-Ar, 250 °C-Ar, 600 °C, and 800 °C samples.[1] The 400 °C sample reaches saturation at significantly lower field and can therefore not be analyzed in the same manner. The magnetization results are analyzed further

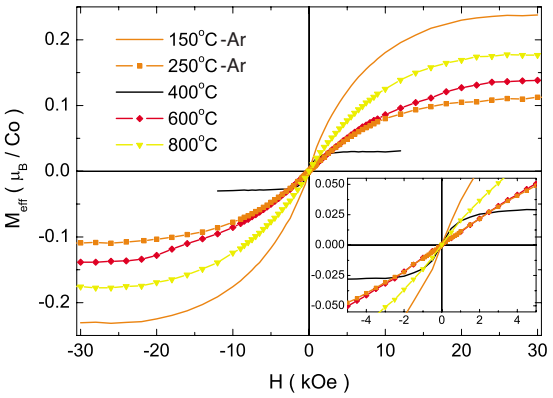

FIG. 1. (Color online) Magnetization (M) versus applied field (H) measured at 2 K. All samples exhibit a paramagneticlike behavior, with no remanent magnetization and zero coercive field. The magnetization of the different samples saturates at some tens of kOe. The exception is the 400 °C sample which saturates at much lower applied field. The inset shows an expanded view of the low-field region for the same curves.

TABLE I. High-field magnetic moments, μ_{HF} (μ_B/Co), obtained from the magnetization at high applied field ($\mu_{\text{HF}}=M_{\text{HF}}/N_T$, where N_T is the number of Co moments per unit volume); effective magnetic moments, $\mu_{\text{eff}}=\sqrt{\frac{\partial M}{\partial H}\cdot\frac{3k_BT}{\mu_0 N_T}}$ (μ_B/Co), derived from the low-field slope of the M versus H curves; n_c is the cluster size, i.e., number of Co atoms and m (μ_B/Co) is the average magnetic moment.

Annealing temperature	μ_{HF}	μ_{eff}	n_c	m
150 °C-Ar	0.24	1.66	48	3.16
250 °C-Ar	0.12	0.97	65	1.95
400 °C	0.031	1.40		
600 °C	0.14	0.98	49	1.87
800 °C	0.18	1.27	50	2.44

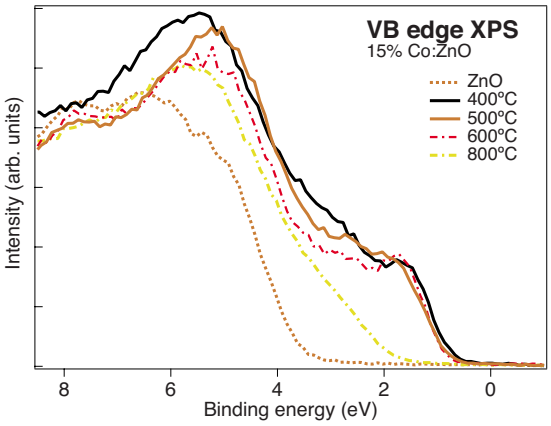

FIG. 2. (Color online) VB XPS recorded using 200 eV photon energy. The 800 °C sample has states at the VB edge where the 3*d* states of substituted Co^{2+} are expected to reside. The 400, 500, and 600 °C samples have additional states in the gap.

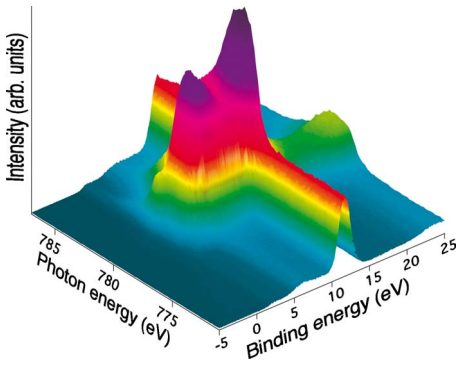

FIG. 3. (Color online) Valence-band RPES spectrum of the 400 °C sample. The valence band was recorded with photon energies ranging across the Co L_3 edge. The Zn 3*d* peak is observed at 12 eV BE. A strong resonance is observed at the VB edge suggesting that the main Co 3*d* contribution is located here. The low BE resonance at 781 eV photon energy is due to the gap states confirming their Co 3*d* character.

at the end of this section after a more complete picture of the chemical composition is obtained from photoemission, x-ray absorption spectroscopy, and XRD.

In Fig. 2 we show the valence band (VB) recorded using 200 eV photon energy. All spectra except the 800 °C spectrum are energy calibrated relative to the Fermi energy (E_F). The 800 °C sample showed indications of charging effects and thus the E_F for this sample could not be determined, instead the Zn 3*d* peaks at 12 eV binding energy (BE) has been aligned between the undoped ZnO and 800 °C sample. The spectra were normalized at 25 eV BE but the intensities should not be compared between spectra due to the lack of an adequate normalization point. Pure ZnO has a direct band gap of 3.4 eV which is approximately the BE of the reference ZnO VB edge. Therefore the conduction-band edge is expected to reside just below 0 eV BE. This suggests that the sample has high intrinsic electron doping mostly due to oxygen vacancies which are common in ZnO. The 800 °C sample has additional states at the VB edge compared to the undoped ZnO. This is where we expect to find the occupied *d* states for substituted Co^{2+} in ZnO.[1] The 400, 500, and 600 °C samples also show additional states in the gap at about 1–2 eV. From the extended valence-band spectrum, also containing the Zn 3*d* peak (not shown), we find that the 500 and 600 °C samples exhibit a shift by about 0.2 eV to lower binding energy relative to the ZnO reference and the 400 °C sample. This indicates that E_F is located further from the conduction band for the 500 and 600 °C samples. There is also an apparent broadening of the 400 °C gap states compared to the 500 and 600 °C samples which could be a delocalization effect as the gap states approaches the ZnO conduction band. The 150 °C-Vac sample is not shown due to large effects on the VB from surface adsorbates. It is however possible to conclude, from the measured spectrum, that there are no gap states present for this sample. Also the 250 °C-Vac sample is not shown since this heat treatment appears to have a severe effect on the electronic structure. It shows metallic states both in Co 2*p* XPS and VB XPS after heating in vacuum. We believe that small amounts of adsorbed organic impurities accumulated on the sample surface is enough to reduce Co into a metallic state when heated in vacuum. For all other samples, the small amount of oxygen present during annealing in Ar atmosphere is enough to suppress the formation of metallic Co.

The valence band was further studied by RPES. The measurements were made by taking the VB photoemission spectra with photon energies ranging across the Co L_3 edge. In a simplified picture one obtains a normal photoemission spectrum of the VB at photon energies below the Co L_3 edge. At resonant photon energies, i.e., close to the Co L_3 absorption edge (cf. Fig. 4), a second channel becomes available where a Co 2*p* electron is excited to an empty Co 3*d* level. When the excited Co atom decays, an Auger electron is emitted from the 3*d* band resulting in final states related to those found in direct photoemission.[17] The Co 3*d* states will therefore be resonantly enhanced in the VB which is shown in Fig. 3, where we show data for the 400 °C sample. The peak observed out of resonance at 12 eV BE is the Zn 3*d* edge. At the VB edge, where we expect the Co^{2+} states to reside, we find a strong resonant enhancement, thus confirming our expectations. Also the Zn 3*d* intensity appears to increase but this effect is dominated by the increase in background at resonant energies. The lowest BE resonance at 781 eV photon energy is very narrow and corresponds to the gap states observed in Fig. 2. This confirms that these states also have a Co 3*d* character.

A total electron yield absorption spectrum is obtained by summing up all the electrons emitted from the sample for every specific photon energy. This spectrum contains information about all the elements which have an absorption edge within that photon energy range. If only electrons within a specific BE range are collected, it is possible to obtain a partial absorption spectrum. This spectrum is restricted to contain information only from species which have VB states at that particular BE. By integrating over a specific BE range in the RPES spectrum we are able to construct a partial absorption spectrum. In Fig. 4 we show a partial Co L_3 absorption spectrum for the 400 °C sample. Similar results were also obtained for the 500 °C sample. The inset shows the

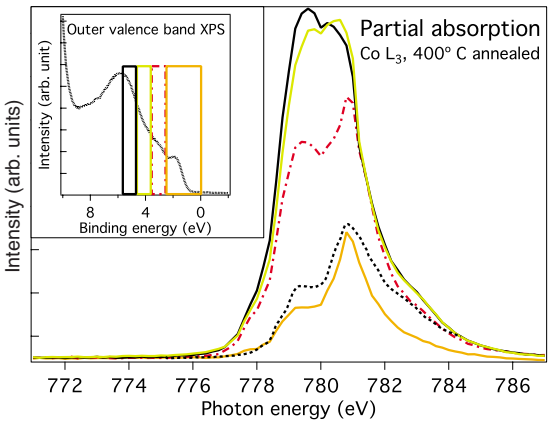

FIG. 4. (Color online) Partial absorption of the Co L_3 edge. The absorption was constructed by integration over specific BE ranges from an RPES spectrum. The inset shows the VB XPS and the boxes indicate which BE ranges have been integrated. When integration is performed for BE$\gtrsim$3 eV the partial absorption is similar to what is expected for Co^{2+} (Refs. 18 and 19). The gap states, i.e., integration with BE$\lesssim$3 eV, have a completely different shape with a sharp peak at 781 eV photon energy. The dashed black line is a reference spectrum of Co_3O_4 obtained from Bazin *et al.* (Ref. 20).

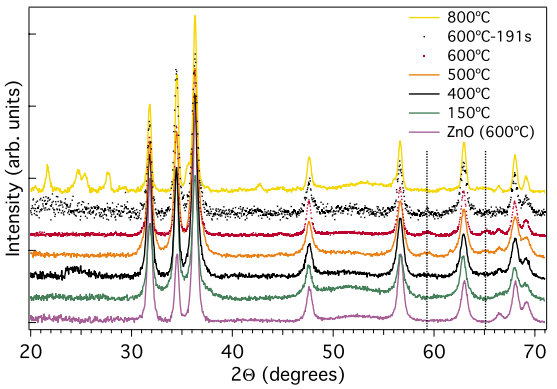

FIG. 5. (Color online) XRD of 15% Co-doped ZnO and reference ZnO. An offset has been applied for clarity and the spectra are stacked in the same order as the legend. Spinel peaks are located around 59° and 65° (black dotted vertical lines) for the 500 and 600 °C samples. The 400 °C sample appears phase pure even though it is very similar to the 600 °C sample in respect to spectroscopy. 600 °C-191 s is an identically prepared sample as the 600 °C but measured with a faster scan rate (191 s/deg).

VB, and the colored boxes show which BE ranges have been integrated. The absorption obtained for BE$\gtrsim$3 eV looks similar to what can be expected for substituted Co^{2+}.[18,19] The absorption obtained for the gap states (BE$\lesssim$3 eV) has a very different shape. Comparing it to the reference spectra of Co_3O_4 (dashed black line in Fig. 4) we can assign the gap states to spinel phase states. The Co_3O_4 spinel structure has one third of the Co atoms in a divalent state which are tetrahedrally coordinated and the remaining Co atoms are in a trivalent state and occupy octahedral positions. The total absorption reference spectrum shown in Fig. 4 is thus a combination of Co^{2+} in tetrahedral coordination, which should give similar absorption structure as substituted Co in ZnO, and Co^{3+} in octahedral coordination which shows the sharp absorption peak at 781 eV photon energy. The similarity to the partial absorption spectra in Fig. 4 indicates that the gap states are due to both Co^{2+} and Co^{3+} final states in the spinel, which is supported by theory.[21,22] The sharp absorption peak at the high photon energy side is also observed in the total electron yield spectra for the 400, 500, and 600 °C samples (not shown).

The Fermi energy is found closest to the ZnO conduction band for the 400 °C sample. The 500 and 600 °C samples have their E_F about 0.2 eV deeper in the band gap. The deepest Fermi energy is presumably found for the 800 °C sample as it was charging during XPS experiments. The location of the E_F is effected by the amount of oxygen vacancies which acts as n dopants in ZnO. Two plausible explanations for the changing E_F are (i) the relative amount of oxygen vacancies in the film decreases with higher annealing temperatures and (ii) the Co^{2+} clusters oxidizing into Co^{3+} results in a reduction in the surrounding ZnO host.

The XRD shown in Fig. 5 confirmed that the 500 and 600 °C samples have traces of spinels observed as peaks at 59° and 65° (black dotted vertical lines). The 400 °C sample which is very similar to the 600 °C sample in respect to spectroscopic measurements still shows a phase pure ZnO structure in XRD. It should also be noted that a weak CoO peak at 42° was found for the 800 °C sample. The spinel structure is not stable at and above 800 °C and decomposes to oxygen and CoO.[23] The sample denoted as 600 °C-191 s is an identically prepared sample as the 600 °C but the XRD data were measured with a faster scan rate (191 s/deg) while all other data shown in Fig. 5 are measured using a scan rate of 764 s/deg. The 600 °C-191 s sample is shown here to illustrate the importance of sufficient statistics since the spinel peak at 59° is vaguely visible while the peak at 65° is in the background noise which initially led us to believe that samples with this concentration and heat treatment could be produced phase pure. The peaks below 30° for the 800 °C sample could not be identified but are believed to be attributed to structures due to a reaction between the film and substrate at high temperatures.

In Fig. 6 we show x-ray photoemission of the spin-orbit split Co $2p_{3/2}$ and $2p_{1/2}$ core levels measured with 1.2 keV photon energy. The spectra are energy calibrated to be aligned at the Zn $3d$ peak. Comparing the background to signal ratio there is a reduction in the signal intensity with higher annealing temperatures (not shown). Only about 1/3 of the signal intensity is left after annealing at 800 °C compared to the as-grown sample which might be an effect of Co diffusing deeper into the ZnO film during the annealing process. The XPS data have been fitted using two different model spectra measured at the high kinetic-energy (HIKE) beamline KMC-1 at the Helmholtz center in Berlin.[24] The high kinetic-energy electrons, obtained by using 3 keV photon energy, measured at HIKE provides a less surface sensitive probe than normal XPS.[1,25] This ensures us that the data are a good representation of bulk properties in the sample. The first model spectrum is 5 at. % Co-doped ZnO which has a Co $2p$ spectrum described as substituted Co^{2+} shown in the top left graph of Fig. 7. Also HIKE data of 35 at. %

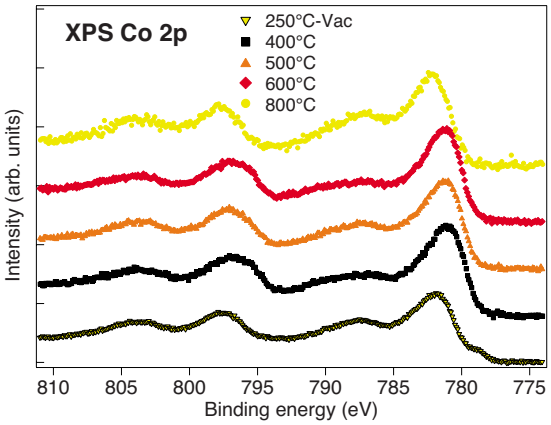

FIG. 6. (Color online) X-ray photoemission of Co $2p$. Spectra were recorded using 1.2 keV photon energy. The intensity of the satellite structures is weaker for samples containing spinel structures than for samples containing only Co^{2+} and there is also a shift to higher BE for the satellites.

Co-doped ZnO annealed in air at 600 °C, top right graph of Fig. 7, which shows a pure Co^{3+} character of cobalt is used as a model. The pure Co^{3+} character can be deduced from the lack of satellite structure 5 eV BE above the Co $2p_{3/2}$ main line which is characteristic for Co^{2+}. This suggests that $ZnCo_2O_4$ which only has Co^{3+} is more stable in this sample than Co_3O_4. The BE difference between the main lines of Co^{2+} and Co^{3+} is small but a good fitting is possible due to the relatively large difference of 0.8 eV in spin-orbit splitting and the large difference in BE and intensity of the satellite structures.[26,27] Both the increase in peak width and spin-orbit splitting of the Co^{2+} component compared to the Co^{3+} component has been described to be an effect of multiplet splitting of the high spin Co^{2+} ($S=3/2$) which is absent for the low spin Co^{3+} ($S=0$).[28–30] The splitting into main and satellite lines are due to different final states after the photoemission of a Co $2p$ core-level electron. In the Co^{2+} spectrum the main lines are due to a $2p^5 3d^8 L^{-1}$ final state, where L^{-1} is a hole in the ligand while the satellites are due to a $2p^5 3d^7 L$ final state.[31] The spectra of the 15% Co-doped samples could be fitted well by using a model consisting of a Co^{3+} spectrum (solid black) and two different types of Co^{2+} spectra [dashed gray (dashed red online) and solid gray (solid orange online] differing only by the BE. The dashed red/gray spectrum which represents Co^{2+} in tetrahedral coordination exists both in the Co_3O_4 spinel and in Co-doped ZnO with Co substituting Zn. The solid orange/gray component which has about 1 eV higher BE is of an uncertain origin but since a good fit is possible by using a BE shifted Co^{2+} component it can be determined to be in a 2+ ionic state. Some possibilities could be Co^{2+} with different amounts of Co neighbors as in the center and on the surface of a Co cluster or Co^{2+} in octahedral coordination as in CoO. The Co $2p$ BE for different Co compounds found in the literature is inconclusive and does not give any insight into the origin of the unknown component. The Co^{3+} peak has 1 eV lower BE than the Co^{2+} (dashed red/gray) which has also been found in other studies.[26,32] Using this model we observe that the relative amount of substitutional Co^{2+} remains constant throughout

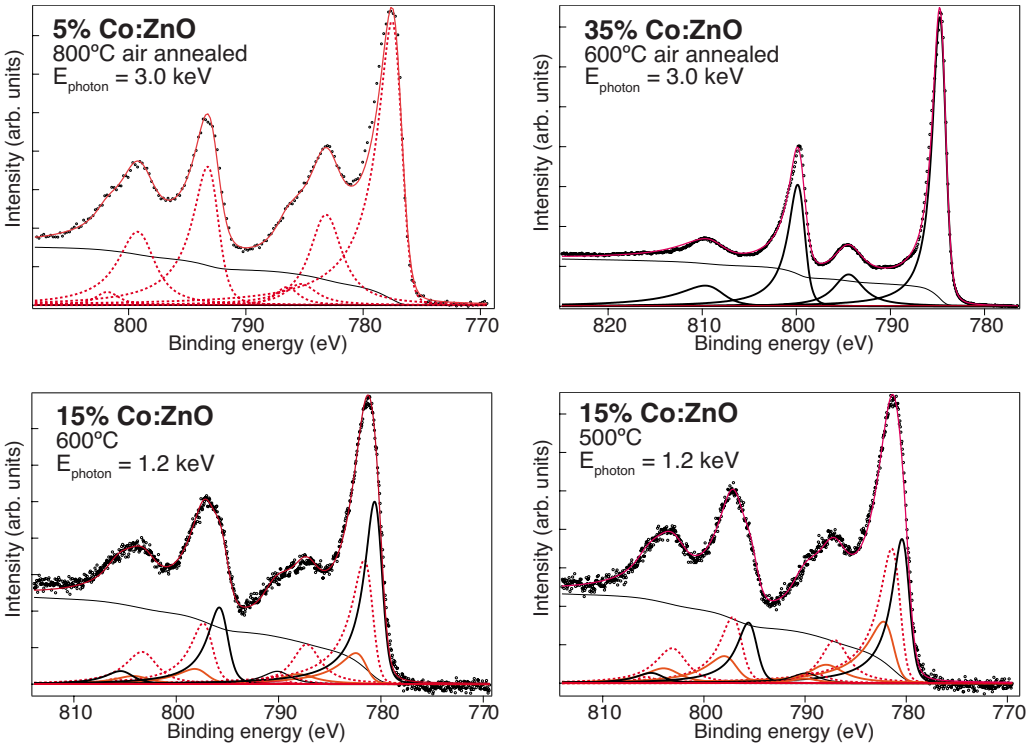

FIG. 7. (Color online) Core-level XPS of Co $2p_{3/2,1/2}$. The top left graph is a low concentration Co-doped ZnO sample and represents the model spectrum of substituted Co^{2+}. Top right graph is a spectrum of a high concentration Co-doped ZnO sample which is used as a model spectrum for pure Co^{3+}. The bottom two graphs are fitted using substituted Co^{2+} (dashed), Co^{3+} (solid black), and an unknown Co^{2+} component [solid gray (orange online)].

the annealing series. Even though the 400 and 600 °C samples are spectroscopically very similar, the 500 °C sample has notably less Co^{3+}, the same effect can be found in Ref. 33. It can also be noted that when the Co^{3+} component increases the unknown Co^{2+} component decreases for all samples.

As it is now evident that there is a significant amount of impurity phases in the samples it is now possible to analyze the magnetic results in a more quantitative way. We have earlier concluded that the magnetic response in these samples is due to uncompensated spins. Using a model described by Néel[34] for antiferromagnetic nanoparticles in which the number of uncompensated spins is proportional to n_c^q, where n_c is the number of Co atoms in the cluster and $q=1/3$ for uncompensated moments randomly distributed on the surface of the cluster. Without making any assumptions about the average magnetic moment of the atoms since the exact chemical composition is unknown, the constraint that μ_{HF} and μ_{eff} should give the same cluster size is employed and we are able to calculate the cluster size (n_c) to be about 50 atoms, see Table I. The n_c is almost constant throughout the annealing series which would suggest that the clusters are produced already during the synthesis of the samples and are only effected chemically during heat treatment. Now that the cluster size is known it is possible to calculate the average magnetic moment (m) of the uncompensated spins which is presented in Table I. For the 150 °C-Ar sample we obtain a magnetic moment of $3.16\mu_B$ which is very close to the expected $3\mu_B$ for Co^{2+}. For intermediate temperatures we obtain a magnetic moment of about $2\mu_B$ which is expected since the Co^{3+} usually obtains a low spin state ($0\mu_B$) and does not contribute to the total magnetic moment. Since the clusters are small it is enough that only the outermost Co layer reacts with the Zn and forms $ZnCo_2O_4$ in order to explain the large amount of Co^{3+} observed. This can also explain why the spinel was not observed in XRD for low annealing temperatures since such a thin layer will have difficulty to relax into a spinel structure unless there is enough thermal energy. Another possibility is that the spinel structure is small enough to be below the detection limit for XRD. The 800 °C sample, which according to XPS should be almost spinel free has a magnetic moment somewhat lower than the expected $3\mu_B$. This might be explained by an evolving geometric structure of the Co clusters during heat treatment. Before annealing the clusters are expected to have approximately spherical geometry which is in good agreement with the magnetization data obtained for the 150 °C-Ar sample. A more energetically favored geometry for clusters of secondary phases should be a layered structure which minimizes the disturbance of the ZnO crystal structure. This would change the value of q, and hence also the magnetic moment, but the calculated cluster size is not affected since it does not depend on q. The most interesting sample is the one annealed at 400 °C. It has a different magnetization versus field shape than the other samples and should not be analyzed using the same model. This sample has a very similar electronic structure as the 600 °C according to XPS except that it seems to have a higher intrinsic n doping. Also, the 400 °C sample showed no indication of spinels in XRD. There are two possible scenarios that can be envisioned. The AFM clusters couple to each other through long-range interaction. If the coupling between the clusters are of both FM and AFM nature, the measured total magnetic moment decreases due to AFM interactions and the saturation field goes down due to FM interactions. This scenario is supported by the observation that the 400 °C sample has a higher n doping and has impurity $3d$ states close to the ZnO conduction band in contrast to the other samples. The impurity $3d$ states also appears broader suggesting that they are less localized. Any long-ranged interaction is expected to be weak which means that the long-ranged AFM interaction is likely to be broken by a high applied field which was not observed for the 400 °C sample. The other possible explanation is that the Co^{3+} containing compound actually obtains a weak ferromagnetic component under certain conditions. It has been shown that the pure Co spinel Co_3O_4 which normally is in an AFM state can exhibit a weak FM behavior when mixed with ZnO.[35] Interesting to note in Ref. 35 is that a hysteresis loop at room temperature was observed for a spinel concentrations of 1% which were not visible in XRD. In Ref. 36 it is found that $ZnCo_2O_4$ which is expected to be nonmagnetic since it only contains low spin Co^{3+} actually shows antiferromagnetism when n doped and ferromagnetism when p doped. The ferromagnetic saturation magnetization as well as the saturation field for p-doped $ZnCo_2O_4$ are of the same order of magnitudes as found for the 400 °C sample.

IV. CONCLUSIONS

Using RPES we have shown that 15 at. % Co-doped ZnO annealed at temperatures between 400 and 600 °C contains a significant amount of Co^{3+} while XRD indicates that the sample annealed at 400 °C is phase pure. It has been shown that Co^{3+} has $3d$ states located in the ZnO host band gap. Most of the samples show a magnetic behavior which can be explained by antiferromagnetic clusters with uncompensated spins. The cluster size is in the order of 50 atoms and the average magnetic moment is reduced when low spin Co^{3+} are formed in the sample. The clusters exist already in the as-prepared sample and the cluster size is not affected by the temperature treatment. The exact composition of the impurity phase is difficult to determine but the $ZnCo_2O_4$ spinel appears to be most stable in ZnO and it also has magnetic properties compatible with the magnetic behavior of all our samples. The sample annealed at 400 °C shows a different magnetic behavior as compared to the other samples and cannot be described by antiferromagnetic clusters alone. A possible explanation is long-range interactions in the sample but a more probable explanation is that impurity phases which have magnetic properties that are very sensitive to doping, heat treatment and chemical surrounding obtain a magnetic behavior at 400 °C which is responsible for the anomalous magnetic behavior.

ACKNOWLEDGMENTS

The authors are grateful to the Swedish Research Council (VR) and the Knut and Alice Wallenberg Foundation (KAW) for financial support.

[1] D. Iuşan, R. Knut, B. Sanyal, O. Karis, O. Eriksson, V. A. Coleman, G. Westin, J. M. Wikberg, and P. Svedlindh, Phys. Rev. B **78**, 085319 (2008).
[2] A. Behan, A. Mokhtari, H. Blythe, D. Score, X.-H. Xu, J. Neal, A. Fox, and G. Gehring, Phys. Rev. Lett. **100**, 047206 (2008).
[3] X. C. Liu, E. W. Shi, Z. Z. Chen, H. W. Zhang, B. Xiao, and L. X. Song, Appl. Phys. Lett. **88**, 252503 (2006).
[4] S. Kuroda, N. Nishizawa, K. Takita, M. Mitome, Y. Bando, K. Osuch, and T. Dietl, Nature Mater. **6**, 440 (2007).
[5] B. Sanyal, R. Knut, O. Granas, D. M. Iusan, O. Karis, and O. Eriksson, J. Appl. Phys. **103**, 07D131 (2008).
[6] J. Coey, Curr. Opin. Solid State Mater. Sci. **10**, 83 (2006).
[7] P. Sharma, A. Gupita, K. Rao, F. Owens, R. Sharma, R. Ahuja, J. Osorio Guillen, B. Johansson, and G. Gehring, Nature Mater. **2**, 673 (2003).
[8] K. Kittilstved, W. Liu, and D. Gamelin, Nature Mater. **5**, 291 (2006).
[9] K. R. Kittilstved, J. Zhao, W. K. Liu, J. D. Bryan, D. A. Schwartz, and D. R. Gamelin, Appl. Phys. Lett. **89**, 062510 (2006).
[10] M. Opel, K.-W. Nielsen, S. Bauer, S. Goennenwein, J. Cezar, D. Schmeisser, J. Simon, W. Mader, and R. Gross, Eur. Phys. J. B **63**, 437 (2008).
[11] A. Ney, M. Opel, T. Kaspar, V. Ney, S. Ye, K. Ollefs, T. Kammermeier, S. Bauer, K.-W. Nielsen, S. Goennenwein, M. Engelhard, S. Zhou, K. Potzger, J. Simon, W. Mader, S. Heald, J. Cezar, F. Wilhelm, A. Rogalev, R. Gross, and S. Chambers, New J. Phys. **12**, 013020 (2010).
[12] K. Rode, R. Mattana, A. Anane, V. Cros, E. Jacquet, J.-P. Contour, F. Petroff, A. Fert, M.-A. Arrio, P. Sainctavit, P. Bencok, F. Wilhelm, N. B. Brookes, and A. Rogalev, Appl. Phys. Lett. **92**, 012509 (2008).
[13] B. Straumal, A. Mazilkin, S. Protasova, A. Myatiev, P. Straumal, and B. Baretzky, Acta Mater. **56**, 6246 (2008).
[14] G. Westin, A. Pohl, M. Ottosson, and K. Jansson, Thin Solid Films **515**, 7751 (2007).
[15] G. Westin, M. Ottoson, and A. Pohl, Thin Solid Films **516**, 4673 (2008).
[16] G. Westin, M. Leideborg, K. Lashgari, V. A. Coleman, K. Jansson, and A. Pohl, Int. J. Nanotechnol. **6**, 828 (2009).
[17] P. A. Brühwiler, O. Karis, and N. Mårtensson, Rev. Mod. Phys. **74**, 703 (2002).
[18] M. Kobayashi, Y. Ishida, J. l. Hwang, T. Mizokawa, A. Fujimori, K. Mamiya, J. Okamoto, Y. Takeda, T. Okane, Y. Saitoh, Y. Muramatsu, A. Tanaka, H. Saeki, H. Tabata, and T. Kawai, Phys. Rev. B **72**, 201201 (2005).
[19] S. Krishnamurthy, C. McGuinness, L. S. Dorneles, M. Venkatesan, J. M. D. Coey, J. G. Lunney, C. H. Patterson, K. E. Smith, T. Learmonth, P. A. Glans, T. Schmitt, and J. H. Guo, J. Appl. Phys. **99**, 08M111 (2006).
[20] D. Bazin, I. Kovács, L. Guczi, P. Parent, C. Laffon, F. D. Groot, O. Ducreux, and J. Lynch, J. Catal. **189**, 456 (2000).
[21] M. A. Langell, M. D. Anderson, G. A. Carson, L. Peng, and S. Smith, Phys. Rev. B **59**, 4791 (1999).
[22] Y. Jugnet and T. M. Duc, J. Phys. Chem. Solids **40**, 29 (1979).
[23] K. N. Hutchings, M. Wilson, P. A. Larsen, and R. A. Cutler, Solid State Ionics **177**, 45 (2006).
[24] M. Gorgoi, S. Svensson, F. Schäfers, G. Öhrwall, M. Mertin, P. Bressler, O. Karis, H. Siegbahn, A. Sandell, H. Rensmo, W. Doherty, C. Jung, W. Braun, and W. Eberhardt, Nucl. Instrum. Methods Phys. Res. A **601**, 48 (2009).
[25] S. Granroth, R. Knut, M. Marcellini, G. Andersson, S. Svensson, O. Karis, M. Gorgoi, F. Schäfers, W. Braun, W. Eberhardt, W. Olovsson, E. Holmström, and N. Mårtensson, Phys. Rev. B **80**, 094104 (2009).
[26] T. Chuang, C. Brundle, and D. Rice, Surf. Sci. **59**, 413 (1976).
[27] H. A. E. Hagelin-Weaver, G. B. Hoflund, D. M. Minahan, and G. N. Salaita, Appl. Surf. Sci. **235**, 420 (2004).
[28] D. Briggs and V. Gibson, Chem. Phys. Lett. **25**, 493 (1974).
[29] D. C. Frost, C. A. McDowell, and I. S. Woolsey, Chem. Phys. Lett. **17**, 320 (1972).
[30] Y. Kolotyrkin, I. Belova, Y. Roginskaya, V. Kozhevnikov, D. Zakhar'in, and Y. Venevtsev, Mater. Chem. Phys. **11**, 29 (1984).
[31] G. A. Carson, M. H. Nassir, and M. A. Langell, J. Vac. Sci. Technol. A **14**, 1637 (1996).
[32] K. Wandelt, Surf. Sci. Rep. **2**, 1 (1982).
[33] Y. K. Lakshmi, K. Srinivas, B. Sreedhar, M. M. Raja, M. Vithal, and P. V. Reddy, Mater. Chem. Phys. **113**, 749 (2009).
[34] L. Néel, C. R. Hebd. Seances Acad. Sci. **252**, 4075 (1961).
[35] A. Quesada, M. A. Garcia, M. Andrés, A. Hernando, J. F. Fernández, A. C. Caballero, M. S. Martin-González, and F. Briones, J. Appl. Phys. **100**, 113909 (2006).
[36] H. J. Kim, I. C. Song, J. H. Sim, H. Kim, D. Kim, Y. E. Ihm, and W. K. Choo, Phys. Status Solidi B **241**, 1553 (2004).